Spatio-Temporal Dynamics of Global Drought

Julio E. Herrera-Estrada[1], Yusuke Satoh[2], Justin Sheffield[1,3]

[1] Department of Civil and Environmental Engineering, Princeton University, Princeton, NJ, USA

[2] International Institute for Applied Systems Analysis, Laxenburg, Austria

[3] Geography and Environment, University of Southampton, Southampton, UK

Corresponding author: Julio Herrera-Estrada (jherrera@princeton.edu)

Key Points:

- Droughts can displace hundreds of kilometers from their origin.

- Several regions experience high mobility and consistent displacement patterns of droughts.

- Droughts tend to lock into further growth and intensification after reaching a certain area and intensity.

Abstract

Understanding the evolution and physical drivers of drought is critical to informing forecasting efforts. One aspect that has seldom been explored is the joint evolution of droughts in space and time. Most studies fix the reference area and focus on their temporal variability, or study their spatial heterogeneity over fixed durations. This work implements a Lagrangian approach by aggregating contiguous areas under drought into clusters. These clusters become the frame of reference and are tracked as they evolve through space and time. Clusters were identified from soil moisture data from the Climate Forecast System Reanalysis (1979-2009). Evapotranspiration, moisture fluxes, and precipitation were used to explore the relevance of possible mechanisms of drought propagation. While most droughts remain near their origin, the centroid of 10% of clusters traveled at least 1,400-3,100 km, depending on the continent. This approach also revealed that large-scale droughts often lock into further growth and intensification.

1. Introduction

Droughts can be deadly and extremely costly [*Sheffield and Wood,* 2011]. Continuous study of these hazards has allowed us to improve our ability to forecast them and develop early-warning systems that provide useful information to agricultural, energy, water, and humanitarian aid sectors. However, we have still failed to predict important droughts, like the one that struck the U.S. Great Plains in the summer of 2012 [*Hoerling et al.,* 2014] and contributed to increases in global food prices [*World Bank,* 2012]. This is partly because we do not yet fully understand how droughts arise, persist, evolve, and recover [*Wood et al.,* 2015]. A contributing factor is how we characterize and analyze droughts' spatio-temporal

dynamics from observations or model predictions.

Previous studies often reduce drought analysis from three dimensions (i.e. latitude, longitude, and time) to one or two [*Lloyd-Hughes,* 2012]. Most have focused on time series analysis of area-averaged variables [see *Mishra and Singh,* 2011, for a review], ignoring conditions in the immediate surroundings of the arbitrary domains, and over upwind regions that are connected to the areas of interest through atmospheric circulation patterns. Few recent studies have analyzed how droughts evolve simultaneously in space and time, by tracking drought clusters – i.e. spatially contiguous areas under drought – and analyzing their characteristics. *Andreadis et al.* [2005] introduced an innovative clustering algorithm to track droughts through space and time along their duration. They used it to introduce Severity-Area-Duration (SAD) curves for the U.S. to assess the spatial variability of droughts of set durations. However, they did not focus on the monthly dynamics themselves. Later studies replicated the SAD curve analysis globally [*Sheffield et al.,* 2009] and for other regions [e.g. *Zhan et al.,* 2016]. Some studies at the country [e.g. *Vicente-Serrano,* 2006; *Vidal et al.*, 2010; *Xu et al.,* 2015; *Zhai et al.* 2016] and continental [*Lloyd-Hughes,* 2012] scales have explored drought cluster characteristics (e.g. distribution of centroids, direction of displacement over time, and changes in cluster area, intensity, and severity). However, the regional scale of these studies still bounds the frame of analysis and prevents a thorough comparison of the spatio-temporal characteristics of drought across the globe. Furthermore, previous studies have been limited to simple assessments of the time series of drought area and intensity [*Vicente-Serrano,* 2006; *Vidal et al.*, 2010; *Gocic et al.,* 2014; *Wang et al.,* 2015], report aggregate regional drought statistics that do not provide insight into the behavior of individual events [*Tallaksen and Stahl*, 2014; *Ge et al.,* 2016].

While the initial onset of droughts is hard to predict, given that it often stems from random atmospheric variability and long-range teleconnections from climatic oscillations [e.g. *Rajagopalan et al.,* 2000; *Giannini et al.,* 2003; *Shabbar and Skinner,* 2004; *Mo and Schemm,* 2008; *Wu and Kinter,* 2009], local and regional feedbacks with the land surface can play a larger role in the subsequent evolution of droughts. Land-atmospheric feedback mechanisms, such as precipitation recycling [e.g. *Rodriguez-Iturbe et al.,* 1991a,b; *Eltahir and Bras,* 1996] have been linked to the intensification and persistence [*Giannini et al.,* 2003; *Wu and Kinter,* 2009; *D'Odorico et al.,* 2013; *Roundy et al.,* 2013], and even propagation of droughts within a continent [*Dominguez et al.,* 2009; *Sheffield et al.,* 2009; *Sheffield and Wood,* 2011]. Thus, in order to understand better how droughts evolve within a region, it is also important to take into account its surroundings, and the regions to which it is atmospherically connected. This can be achieved by carrying out joint spatio-temporal analysis of droughts that provides a more complete picture of their development beyond their origin. Increased understanding of the relevant local and regional land-atmospheric feedbacks that this approach would bring, may inform the physical processes that need to be improved in climate models to help advance predictive capabilities.

Here we use a Lagrangian approach where individual drought events become the frame of reference, providing unique insights into the spatio-temporal dynamics of droughts. Several characteristics of drought behavior are proposed and analyzed, including how droughts displace across continents and their monthly patterns of growth, intensification, and recovery. The statistics of these characteristics are aggregated to the continental scale and compared globally to evaluate regional differences in drought behavior. Droughts are defined based on soil moisture from reanalysis data. Furthermore, to study the extent to which drought displacements occur downwind through reductions of moisture exports, anomalies in

evapotranspiration (ET), moisture fluxes (MF), and precipitation (Prcp) along the clusters'

tracks are analyzed. We hypothesize that the drought dynamics analyzed here are driven by a

combination of atmospheric drivers, land-atmosphere feedbacks, and geographic factors,

including merging and splitting of individual droughts. In this study, we explore the spatio-

temporal characteristics of droughts in a systematic way as a first step to understanding the

mechanisms of their development, persistence, and displacement.

2. Material and Methods

We used data from the Climate Forecast System Reanalysis (CFSR) to identify areas under

drought using a percentile threshold definition. Contiguous regions under drought were

aggregated into clusters, and tracked over time and space. Characteristics of the clusters were

calculated and compared across continental regions.

2.1. Data and Definitions

Monthly 2-meter soil moisture, Prcp, latent heat flux, and tropospheric (1000mb-250mb)

wind and specific humidity data from CFSR at 0.5-degree resolution from 1979-2009 was

used. Latent heat flux was used as a proxy for evapotranspiration, so it is referred to as ET

henceforth. CFSR is a state-of-the art reanalysis that has been used for land-surface

hydrology research [e.g. *Mo et al.,* 2011; *Meng et al.,* 2012] and has been identified to

generally reproduce observed droughts more accurately than other reanalysis datasets [*Zhan

et al.,* 2016]. We focus on agricultural droughts calculated from soil moisture, given its

importance for vegetation, agricultural productivity, and for controlling relevant land-

atmospheric interactions.

For each variable, percentiles are first calculated from the empirical cumulative distribution function of each month. Individual values are replaced by their respective percentiles, and droughts are defined when these are under a given threshold. The 15th percentile was chosen since it approximates the threshold of common drought metrics, like the Standardized Precipitation Index or Palmer Drought Severity Index value of -1 [*Guttman,* 1999; *Szép et al.,* 2005]. This definition allows a direct comparison of dry anomalies across regions with different climates, permitting the study of drought dynamics throughout each continent. This could not be done by using an absolute value threshold.

Drought metrics used here are defined in Equations 1-3:

$$I_j(t) = 1 - P_j(t) \tag{1}$$

$$\bar{I}(t) = \frac{1}{n} \sum_{j=1}^{n} I_j(t) \tag{2}$$

$$S = \sum_{t=1}^{D} \bar{I}(t) \tag{3}$$

where $I_j(t)$ is the intensity during month t in grid-cell j, $P_j(t)$ is the percentile during month t in grid-cell j, $\bar{I}(t)$ is the mean intensity of a cluster during month t, n is the number of grid-cells in the cluster at time t, S is the cluster's severity, and D is the cluster's duration. Intensity is defined such that lower percentiles represent higher intensities.

2.2. Clustering Algorithm

The clustering methodology follows *Andreadis et al.* [2005]. After percentiles are calculated and the threshold is implemented at each grid-cell, a 2-D median filter is applied to each monthly map to smooth out spatial noise. Contiguous grid-cells under drought are then aggregated into clusters. Clusters smaller than 200,000 km^2 are filtered out following *Andreadis et al.* [2005] and *Sheffield et al.* [2009], focusing the analysis on large-scale droughts that have higher likelihood of persisting and displacing. The cluster centroids are found using a weighted center of intensity where the intensity values of the cluster grid-cells are used as weights.

Drought events were tracked through time by searching for overlapping grid-cells between clusters at contiguous time steps. The tracking algorithm records if a cluster splits, merges, or does both at the same time. Droughts over Greenland, and those whose centroids fell within the Sahara Desert (20N-25N, 17W-34E) were removed from the analysis, since droughts in these regions were not of interest for this study. Clusters were allowed to propagate into the Sahara until their centroids fell within the described domain.

2.4. Spatial and Statistical Analysis

The drought cluster centroids generate tracks throughout the continents as they displace from month to month. To understand the characteristics of these tracks and whether there are certain regions that experience higher drought displacement, a map of 10-by-10-degree grid-cells was generated and the number of tracks within each grid-cell was counted. By calculating the number of tracks within these larger grid-cells, we obtain a better

representation of regions with frequent drought clusters displacing through them. Only monthly displacements with magnitude of 150 km or more were considered to avoid counting small displacements that would fall within the uncertainty of the cluster centroid location. Instances when clusters merged or split were ignored because these result in large changes in the centroid's location. Furthermore, the displacement vector of unit-length of each drought cluster was recorded each time a cluster passed through one of these grid-cells. The centroids' displacements were also sorted into three categories: 1-2) displacement due to asymmetric growth or shrinkage, and 3) displacement of the entire cluster. To categorize centroid displacements, the overlap in the number of grid-cells in a cluster between two time steps was calculated. If the overlap was equal or larger than 75%, the cluster was considered to have grown or shrunk asymmetrically. This distinction was determined by comparing the cluster areas between time steps. Otherwise, the cluster was determined to have moved locations.

Seven cluster characteristics were evaluated: 1) duration, 2) distance between cluster centroids at the start and at subsequent time steps (i.e. monthly displacement), 3-4) cluster areas and mean intensities (Equation 2) at each time step, 5) cluster severity at each time step (Equation 3), and 6-7) rate of change in cluster area and mean intensity between time steps. These represent a range of different drought characteristics and dynamics.

Characteristics 1-5 were calculated at every time step for each cluster and their statistics were aggregated for six continental regions (North America, South America, Europe, Africa, Asia, and Australia). For each region, the complementary conditional distribution functions (CCDF) of the clusters' displacement, maximum area, and severity reaching at least a given threshold value conditional on a range of durations were calculated. The two chosen

thresholds values corresponded to the means across regions of the 50th and 80th percentiles of each characteristic for droughts that had lasted two years or less (since observations decreased in several regions for longer-lasting clusters). The median durations of clusters that reached a range of displacements were also calculated.

For each region, the rates of change in area were calculated each month as a function of cluster area in the previous month. Instances when clusters merged or split were discarded, since this often caused large area changes. A 2-D histogram was generated from the scatter plot of rates of change in area against cluster area in the previous month, with 10 bins dividing each axis. Linear regressions were calculated to model how rates of change in area vary as a function of cluster area. This was repeated to model the rates of change in mean intensity as a function of the clusters' mean intensities in the previous month.

A possible mechanism of drought propagation is the reduction of MF downwind caused by reduced ET over an area under drought. This reduction of moisture exports can then lead to decreased Prcp over a region downwind [*Dominguez et al.,* 2009]. To do a first approximation of the relevance of this mechanism, vertically integrated MF (1000mb-250mb) were calculated from monthly data.

To find pairs of regions that have been under drought and are atmospherically connected, disjoint domains R1 and R2 occupied by the same drought cluster at two different points in time t_1 and t_2 ($t_1 < t_2$), respectively, were identified. A linear boundary was drawn at the mid-point between the centroids of R1 and R2 (see Figure 4(a)), and the length of the boundary was set to the diameter of a circle with an area equal to the mean of the areas of the two domains. The MF perpendicular to the boundary in the direction from R1 to R2 was

calculated for every month between 1979-2009. If this was positive, then R2 was determined

to be downwind from R1. For these cases, Spearman rank correlations ρ were calculated

between monthly time series (1979-2009) of ET anomalies averaged over R1 and the time

series of MF anomalies crossing the boundary towards R2, and between the time series of MF

anomalies and the time series of Prcp anomalies averaged over R2. If this pair of correlations

was positive and statistically significant (p<0.05, the reduction of moisture exports was

determined to be a contributing mechanism (but not necessarily the only one) to the

propagation of that cluster. This was repeated for each cluster by finding R1 and R2 using

$t_1=0$ and $t_2=2D/3$, and $t_1=D/3$ and $t_2=D$, where D is the cluster's total duration, and making

sure there was no overlap between any combination of domains.

3. Results

3.1. Spatial Patterns of Drought Displacement

A total of 1,420 drought clusters were identified, and their centroids were tracked throughout

the world. Figure 1(a) shows selected contours and the track of an example cluster that

displaced from California to the U.S. Great Plains. Figure 1(b) shows the tracks of drought

clusters over North America that lasted at least 3 months and travelled at least 500 km. A

map of the track densities in an upscaled grid of 10-by-10 degrees was generated and is

displayed in Figure 1(c). This shows "hotspots" of cluster tracks in the southeast of the

United States, northwest of Mexico, northwest of Brazil, south of Brazil and north of

Argentina, Central and Eastern Europe, Central Africa, northwest of India, Southeast Asia,

and Australia. These areas cover tropical, temperate, and semi-arid climates, suggesting that

there are a variety of factors involved in drought displacement within each region. Note that

despite some regions experiencing prolonged drought between 1979-2009 (e.g. the Sahel), these droughts are not necessarily frequently mobile. This is potentially because atmospheric pressure patterns in these regions are more stable, and because these regions may not be important sources of moisture for other areas downwind, preventing the drought signal from propagating farther through reduced moisture exports [e.g. *Giannini et al.,* 2003; *Keys et al.,* 2014; *Arnault et al.,* 2016].

Figure 1(c) also shows a vector field of the drought clusters' net displacement for each 10-by-10-degree grid-cell. Longer arrows indicate that several clusters followed the same direction. Conversely, short arrows or their absence indicate that there were no regional coherent displacement patterns (e.g. clusters moved eastwards almost as frequently as they moved westwards). The longest arrows are found in South America and Australia. For Europe, the lack of arrows is partially due to the smaller number of droughts in the region given the continent's smaller size.

Depending on the region, asymmetric growth was responsible for 10-23% of centroid displacements, asymmetric shrinkage for 13-32%, and cluster displacement for 49-76%. Asymmetric shrinking is more frequent than asymmetric growth since storms can quickly relieve a section of the cluster from drought conditions [e.g. *Kam et al.,* 2013]. Europe and Australia experience the highest proportion of cluster displacement (76% and 58%, respectively); North America and Asia the highest proportion of asymmetric growth (23% and 22%, respectively); and North America, South America, and Africa of asymmetric shrinkage (25%, 25%, and 32%, respectively). The patterns of motion in Figure 1(c) combine the direction that droughts follow when they displace, as well as the direction in which they grow and shrink. As droughts shrink their centroid may move in the opposite direction in

which they grew, suggesting that these displacements could be analyzed further based on the season and the timing of the drought, though the lack of samples makes this challenging.

3.2. Spatio-Temporal Characteristics

Figures 2(a-f) display the CCDF of displacement, maximum area, and severity reaching at least two different thresholds, conditional on a range of cluster durations for each region. Australian, South American, and European clusters have higher probabilities of displacing further for each duration, while African and North American clusters tend to be more static in comparison. South American and European clusters also have higher probabilities of growing beyond 1 and 2 million km^2, while North American, African, and Australian droughts tend to be smaller. Most regions display similar probabilities of clusters reaching the given severity thresholds, except for North America, where droughts tend to be less severe, comparatively. Figure 2(g) shows the median durations that it took clusters to reach a range of displacements. They suggest that South American and Asian clusters tend to have faster displacements, and African and Australian clusters slower ones. This shows that although droughts appear to displace everywhere in the world, there are distinct regional differences in their behaviors month-to-month.

Monthly rates of change of area and mean intensity were calculated for clusters of different areas and mean intensities, respectively. Figure 3 shows the resulting 2-D histograms and linear regressions. The high frequencies in the 2-D histogram for smaller areas imply that smaller clusters (that are still larger than 200,000 km^2) have a higher propensity of growing further. Conversely, very large clusters located in the middle and right end of the x-axis tend to shrink instead. The histograms of the clusters' intensities show higher frequencies of

positive changes for less intense droughts (that have reached dry anomaly of the 15th percentile), and higher frequencies of negative changes for more intense droughts. This implies that less intense droughts tend to intensify further. The negative correlations from the linear regressions support these conclusions. The dynamics shown here may be partially due to local positive feedbacks (e.g. precipitation recycling) that lock clusters into drought conditions making it harder for recovery to take place [e.g. *Giannini et al.,* 2003; *Wu and Kinter,* 2009; *D'Odorico et al.,* 2013; *Roundy et al.,* 2013].

3.3. Role of Moisture Exports Reduction on Drought Propagation

Disjoint domains from the same clusters were used to identify regions that are atmospherically connected, and to study the contributions of anomalies of moisture exports on drought propagation. Figure 4(a) shows example domains R1 and R2 as described in Section 2.4 for the cluster in Figure 1(a). Figure 4(b) displays the scatter plot and Spearman ρ between the monthly time series (1979-2009) of ET anomalies averaged over R1 and the MF anomalies across the boundary in the direction of R2 in 4(a). Similarly, Figure 4(c) shows the relationship between MF anomalies across the boundary and Prcp anomalies averaged over R2. Since these two correlations were positive and significant, and the mean flux across the boundary towards R2 was positive (not shown) we conclude that reduction of moisture exports from R1 can influence drought propagation into R2 for this pair of domains.

This analysis was repeated for 60 pairs of disjoint domains in total, globally, and R2 was determined to be downwind from R1 in 42 of them. Figure 4(d) shows the histograms of Spearman ρ's between ET anomalies and MF anomalies for those 42 cases, and 4(e) the Spearman ρ's between MF anomalies and Prcp anomalies. The shaded red bars correspond to

the cases for which moisture exports were found to have made a contribution to drought propagation as defined above. Figure 4(f) displays the percentage of domain pairs for which reduction of moisture exports were found to be a contributing factor for drought propagation in each region, including all pairs. North and South America had the highest proportion (45% and 27%, respectively), while Australia and Asia had the lowest (0% and 10%, respectively). These results suggest that regional land-atmospheric feedbacks may play a role in drought propagation at the large, sub-continental spatial scales considered in this study, though other atmospheric mechanisms are also important. This is a first-order analysis that considers predominant MF at the monthly scale, but further work should be done using MF derived at higher temporal resolutions.

4. Discussion and Conclusions

CFSR data was used here to identify drought clusters and characterize their monthly spatio-temporal dynamics across the world. This work advances our current understanding of drought dynamics, showing that drought clusters can displace hundreds of kilometers in every continent, sometimes partially due to the reduction of moisture exports that propagate the drought signal downwind. While these traveling droughts might only represent a small fraction of the total number of events, they are likely to have some of the largest societal impacts given that they are also the longest lasting and most severe ones.

This analysis draws a parallel with tropical cyclone studies, in which the densities and directions of their tracks have been analyzed in the world's oceans [*Zhao et al.,* 2009]. Similarly, there are hotspots where more droughts pass through and common directions that they tend to follow over various land-regions around the world.

The drought clusters' displacements and their area and intensity dynamics suggest that land-atmospheric feedback mechanisms, such as precipitation recycling might play an important role in the evolution of droughts, both locally and downwind [e.g. *Dominguez et al.,* 2009; *Roundy et al.,* 2013]. This is in addition to other atmospheric phenomena, such as the displacement of high-pressure systems, and heightened probability of drought over large areas due to teleconnections with sea surface temperatures. Results shown here also suggest the existence of area and intensity thresholds beyond which it is more likely for droughts to grow and intensify before they recover.

Improved understanding of the physical mechanisms behind the spatio-temporal dynamics of droughts explored here highlights areas in which forecast models should be improved. Combining the approach presented in this work with increased understanding of the physical mechanisms may enable the development of statistical-physical models of drought clusters that can be used for risk assessment and seasonal forecasting, similar to those for tropical cyclones [e.g. *Yonekura and Hall*, 2011].

The ability of droughts to displace across regions also poses important implications for regional cooperation and information exchange between governments at different scales (e.g. municipal, state, and national) regarding drought risk mitigation and management. An example of this is the North American Drought Monitor, which links information between Mexico, the U.S. and Canada [*Lawrimore et al.,* 2002]. These information systems can help stakeholders make appropriate decisions to mitigate droughts' impacts before they displace into their region and throughout the droughts' development.

5. Acknowledgements

References

Andreadis, K. M., E. A. Clark, A. W. Wood, A. F. Hamlet, and D. P. Lettenmaier (2005), Twentieth-century drought in the conterminous United States, *Journal of Hydrometeorology*, *6*(6), 985–1001, doi: 10.1175/JHM450.1.

Arnault, J., R. Knoche, J. Wei, and H. Kunstmann (2016), Evaporation tagging and atmospheric water budget analysis with WRF: A regional precipitation recycling study for West Africa, *Water Resour. Res.*, *52*(3), 1544–1567, doi:10.1002/2015WR017704.

D'Odorico, P., A. Bhattachan, K. F. Davis, S. Ravi, and C. W. Runyan (2013), Global desertification: Drivers and feedbacks, *Advances in Water Resources*, *51*, 326–344, doi:10.1016/j.advwatres.2012.01.013.

Dominguez, F., J. C. Villegas, and D. D. Breshears (2009), Spatial extent of the North American Monsoon: Increased cross-regional linkages via atmospheric pathways:

ATMOSPHERIC HYDROLOGIC CONNECTIVITY, *Geophysical Research Letters*, *36*(7), n/a–n/a, doi:10.1029/2008GL037012.

Eltahir, E. A. B., and R. L. Bras (1996), Precipitation recycling, *Rev. Geophys.*, *34*(3), 367–378, doi:10.1029/96RG01927.

Ge, Y., T. Apurv, and X. Cai (2016), Spatial and temporal patterns of drought in the Continental U.S. during the past century, *Geophys. Res. Lett.*, *43*(12), 2016GL069660, doi:10.1002/2016GL069660.

Giannini, A., R. Saravanan, and P. Chang (2003), Oceanic Forcing of Sahel Rainfall on Interannual to Interdecadal Time Scales, *Science*, *302*(5647), 1027–1030, doi:10.1126/science.1089357.

Gocic, M., and S. Trajkovic (2014), Spatiotemporal characteristics of drought in Serbia, *Journal of Hydrology*, *510*, 110–123, doi:10.1016/j.jhydrol.2013.12.030.

Guttman, N. B. (1999), Accepting the Standardized Precipitation Index: A Calculation Algorithm1, *JAWRA Journal of the American Water Resources Association*, *35*(2), 311–322, doi:10.1111/j.1752-1688.1999.tb03592.x.

Hoerling, M., J. Eischeid, A. Kumar, R. Leung, A. Mariotti, K. Mo, S. Schubert, and R. Seager (2014), Causes and Predictability of the 2012 Great Plains Drought, *Bull. Amer. Meteor. Soc.*, *95*(2), 269–282, doi:10.1175/BAMS-D-13-00055.1.

Kam, J., J. Sheffield, X. Yuan, and E. F. Wood (2013), The Influence of Atlantic Tropical Cyclones on Drought over the Eastern United States (1980–2007), *J. Climate*, *26*(10), 3067–3086, doi:10.1175/JCLI-D-12-00244.1.

Keys, P. W., E. A. Barnes, R. J. van der Ent, and L. J. Gordon (2014), Variability of moisture

recycling using a precipitationshed framework, *Hydrol. Earth Syst. Sci.*, *18*(10), 3937–3950, doi:10.5194/hess-18-3937-2014.

Lawrimore, J., R. R. Heim, M. Svoboda, V. Swail, and P. J. Englehart (2002), Beginning a New Era of Drought Monitoring Across North America, *Bull. Amer. Meteor. Soc.*, *83*(8), 1191–1192, doi:10.1175/1520-0477(2002)083<1191:BANEOD>2.3.CO;2.

Lloyd-Hughes, B. (2012), A spatio-temporal structure-based approach to drought characterisation, *International Journal of Climatology*, *32*(3), 406–418, doi:10.1002/joc.2280.

Meng, J., R. Yang, H. Wei, M. Ek, G. Gayno, P. Xie, and K. Mitchell (2012), The Land Surface Analysis in the NCEP Climate Forecast System Reanalysis, *J. Hydrometeor.*, *13*(5), 1621–1630, doi:10.1175/JHM-D-11-090.1.

Mishra, A. K., and V. P. Singh (2011), Drought modeling – A review, *Journal of Hydrology*, *403*(1-2), 157–175, doi:10.1016/j.jhydrol.2011.03.049.

Mo, K. C., and J. E. Schemm (2008), Droughts and Persistent Wet Spells over the United States and Mexico, *J. Climate*, *21*(5), 980–994, doi:10.1175/2007JCLI1616.1.

Mo, K. C., L. N. Long, Y. Xia, S. K. Yang, J. E. Schemm, and M. Ek (2011), Drought Indices Based on the Climate Forecast System Reanalysis and Ensemble NLDAS, *J. Hydrometeor.*, *12*(2), 181–205, doi:10.1175/2010JHM1310.1.

Rajagopalan, B., E. Cook, U. Lall, and B. K. Ray (2000), Spatiotemporal Variability of ENSO and SST Teleconnections to Summer Drought over the United States during the Twentieth Century, *J. Climate*, *13*(24), 4244–4255, doi:10.1175/1520-0442(2000)013<4244:SVOEAS>2.0.CO;2.

Rodriguez-Iturbe, I., D. Entekhabi, and R. L. Bras (1991a), Nonlinear Dynamics of Soil
Moisture at Climate Scales: 1. Stochastic Analysis, *Water Resour. Res.*, *27*(8), 1899–
1906, doi:10.1029/91WR01035.

Rodriguez-Iturbe, I., D. Entekhabi, J.-S. Lee, and R. L. Bras (1991b), Nonlinear Dynamics of
Soil Moisture at Climate Scales: 2. Chaotic Analysis, *Water Resour. Res.*, *27*(8),
1907–1915, doi:10.1029/91WR01036.

Roundy, J. K., C. R. Ferguson, and E. F. Wood (2013), Temporal Variability of Land–
Atmosphere Coupling and Its Implications for Drought over the Southeast United
States, *J. Hydrometeor*, *14*(2), 622–635, doi:10.1175/JHM-D-12-090.1.

Seneviratne, S. I., T. Corti, E. L. Davin, M. Hirschi, E. B. Jaeger, I. Lehner, B. Orlowsky, and
A. J. Teuling (2010), Investigating soil moisture–climate interactions in a changing
climate: A review, *Earth-Science Reviews*, *99*(3-4), 125–161,
doi:10.1016/j.earscirev.2010.02.004.

Shabbar, A., and W. Skinner (2004), Summer Drought Patterns in Canada and the
Relationship to Global Sea Surface Temperatures, *J. Climate*, *17*(14), 2866–2880,
doi:10.1175/1520-0442(2004)017<2866:SDPICA>2.0.CO;2.

Sheffield, J., K. M. Andreadis, E. F. Wood, and D. P. Lettenmaier (2009), Global and
Continental Drought in the Second Half of the Twentieth Century: Severity–Area–
Duration Analysis and Temporal Variability of Large-Scale Events, *Journal of
Climate*, *22*(8), 1962–1981, doi:10.1175/2008JCLI2722.1.

Sheffield, J., and E. F. Wood (2011), Drought: Past Problems and Future Scenarios, London:
Earthscan, Print.

Szép, I. J., J. Mika, and Z. Dunkel (2005), Palmer drought severity index as soil moisture

indicator: physical interpretation, statistical behaviour and relation to global climate,

Physics and Chemistry of the Earth, Parts A/B/C, *30*(1-3), 231–243,

doi:10.1016/j.pce.2004.08.039.

Tallaksen, L. M., and K. Stahl (2014), Spatial and temporal patterns of large-scale droughts

in Europe: Model dispersion and performance: Tallaksen and Stahl: Large-scale

hydrological droughts, *Geophysical Research Letters*, *41*(2), 429–434,

doi:10.1002/2013GL058573.

Vicente-Serrano, S. M. (2006), Differences in Spatial Patterns of Drought on Different Time

Scales: An Analysis of the Iberian Peninsula, *Water Resources Management*, *20*(1),

37–60, doi:10.1007/s11269-006-2974-8.

Vidal, J.-P., E. Martin, L. Franchistéguy, F. Habets, J.-M. Soubeyroux, M. Blanchard, and M.

Baillon (2010), Multilevel and multiscale drought reanalysis over France with the

Safran-Isba-Modcou hydrometeorological suite, *Hydrol. Earth Syst. Sci.*, *14*(3), 459–

478, doi:10.5194/hess-14-459-2010.

Wang, K., Q. Li, Y. Yang, M. Zeng, P. Li, and J. Zhang (2015), Analysis of spatio-temporal

evolution of droughts in Luanhe River Basin using different drought indices, *Water

Science and Engineering*, *8*(4), 282–290, doi:10.1016/j.wse.2015.11.004.

Wood, E. F., S. D. Schubert, A. W. Wood, C. D. Peters-Lidard, K. C. Mo, A. Mariotti, and R.

S. Pulwarty (2015), Prospects for Advancing Drought Understanding, Monitoring,

and Prediction, *J. Hydrometeor.*, *16*(4), 1636–1657, doi:10.1175/JHM-D-14-0164.1.

World Bank, 2012: Food Price Watch – August 2012, Washington, DC: The World Bank.

Online. Accessed October 5, 2016.

Wu, R., and J. L. Kinter (2009), Analysis of the Relationship of U.S. Droughts with SST and Soil Moisture: Distinguishing the Time Scale of Droughts, *Journal of Climate*, *22*(17), 4520–4538, doi:10.1175/2009JCLI2841.1.

Xu, K., D. Yang, H. Yang, Z. Li, Y. Qin, and Y. Shen (2015), Spatio-temporal variation of drought in China during 1961–2012: A climatic perspective, *Journal of Hydrology*, *526*, 253–264, doi:10.1016/j.jhydrol.2014.09.047.

Yonekura, E., and T. M. Hall (2011), A Statistical Model of Tropical Cyclone Tracks in the Western North Pacific with ENSO-Dependent Cyclogenesis, *J. Appl. Meteor. Climatol.*, *50*(8), 1725–1739, doi:10.1175/2011JAMC2617.1.

Zhan, W., K. Guan, J. Sheffield, and E. F. Wood (2016), Depiction of drought over sub-Saharan Africa using reanalyses precipitation data sets, *J. Geophys. Res. Atmos.*, *121*(18), 2016JD024858, doi:10.1002/2016JD024858.

Zhai, J., J. Huang, B. Su, L. Cao, Y. Wang, T. Jiang, and T. Fischer (2016), Intensity–area–duration analysis of droughts in China 1960–2013, *Clim Dyn*, 1–18, doi:10.1007/s00382-016-3066-y.

Zhao, M., I. M. Held, S.-J. Lin, and G. A. Vecchi (2009), Simulations of Global Hurricane Climatology, Interannual Variability, and Response to Global Warming Using a 50-km Resolution GCM, *J. Climate*, *22*(24), 6653–6678, doi:10.1175/2009JCLI3049.1.
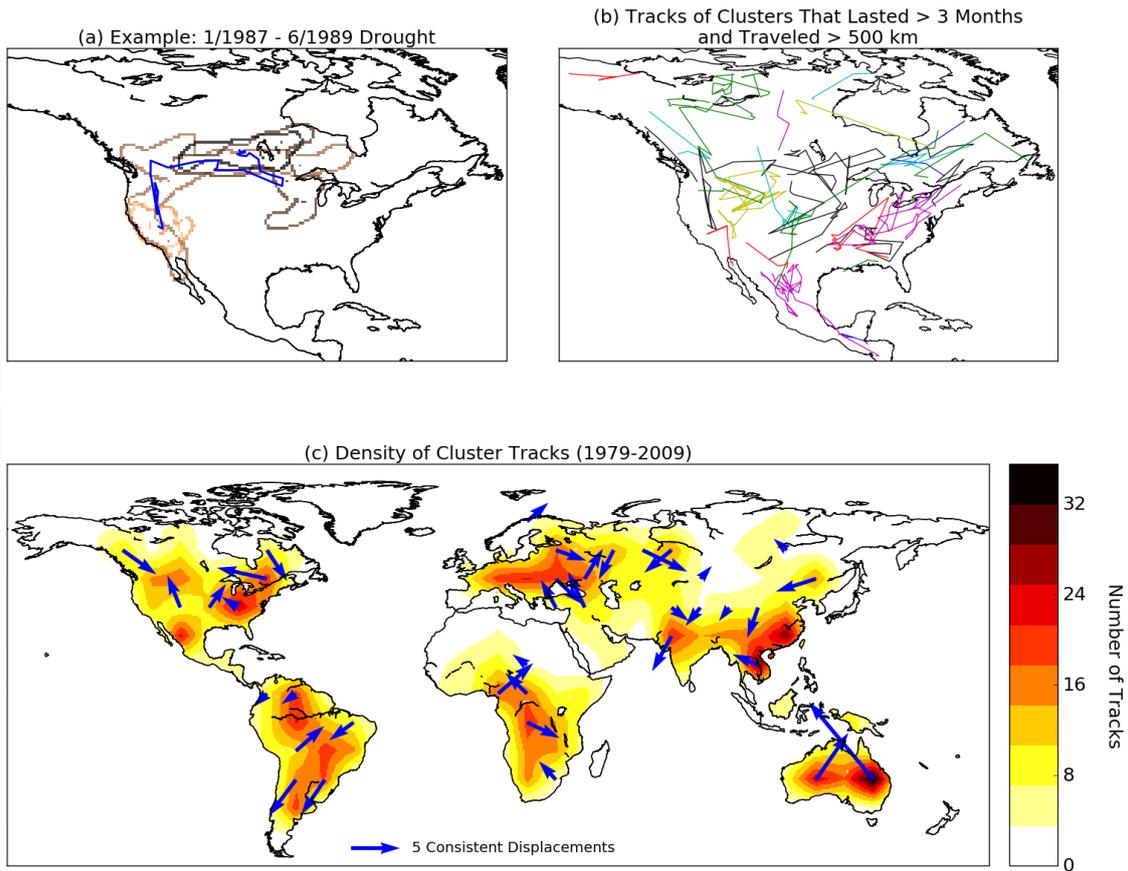
Figure 1. (a) Example of a soil moisture drought cluster. Darker contours show later domains occupied by the cluster. The blue line represents the cluster centroid's track. (b) Drought cluster tracks that displaced at least 500 km and lasted at least 3 months over North America. (c) Density of tracks around the world. Blue arrows represent net direction of droughts passing through.
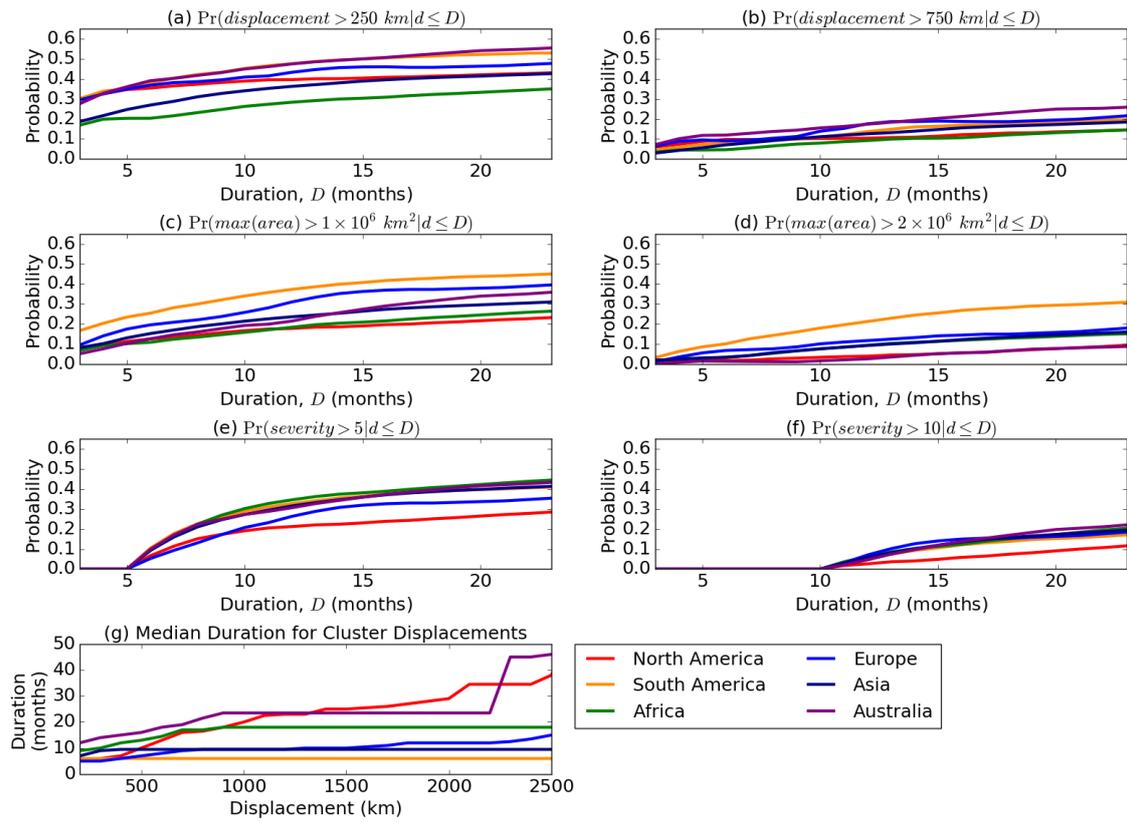
Figure 2. CCDFs of (a-b) displacements, (c-d) maximum areas, (e-f) and severities exceeding two thresholds, conditional on a range of durations, for each region. (g) Median duration of clusters that have reached a range of displacements in each region.
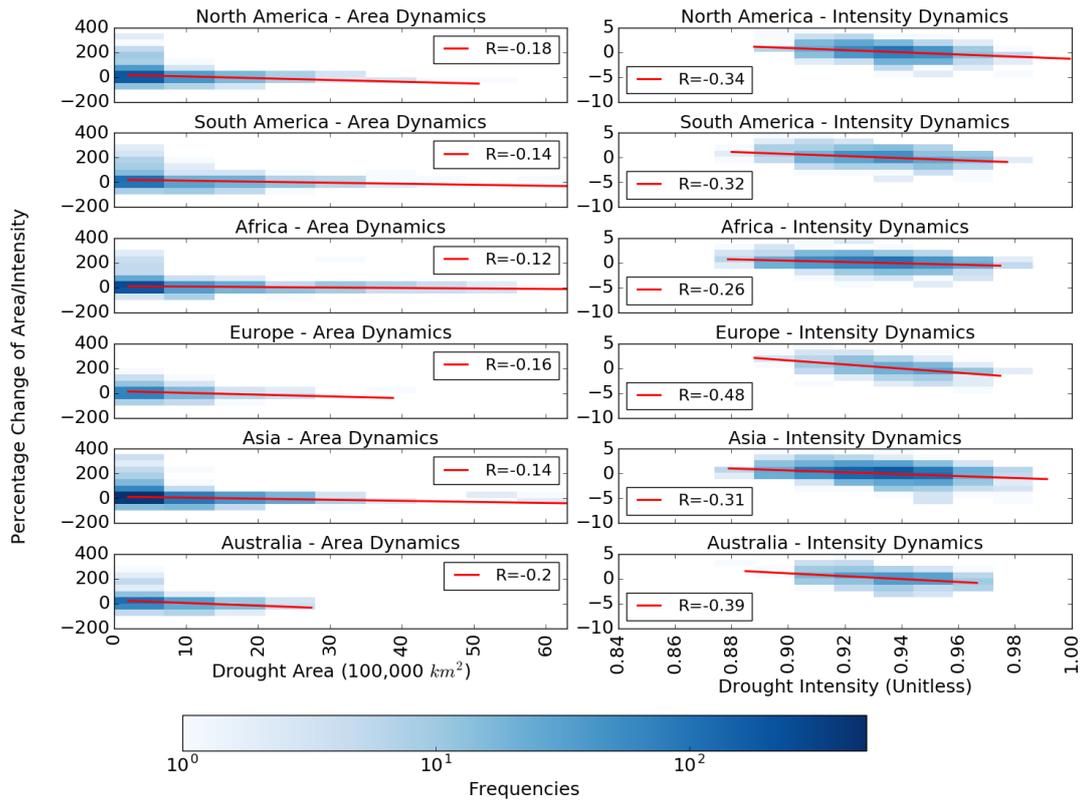
Figure 3. Regional 2-D histograms of rates of change in area (left) and intensity (right) as a function of area and intensity, respectively, during the previous month. Red line displays linear regression results. All correlations yielded p<0.05.

Estimated Regional Contribution of Reduced Moisture Exports on Drought Propagation
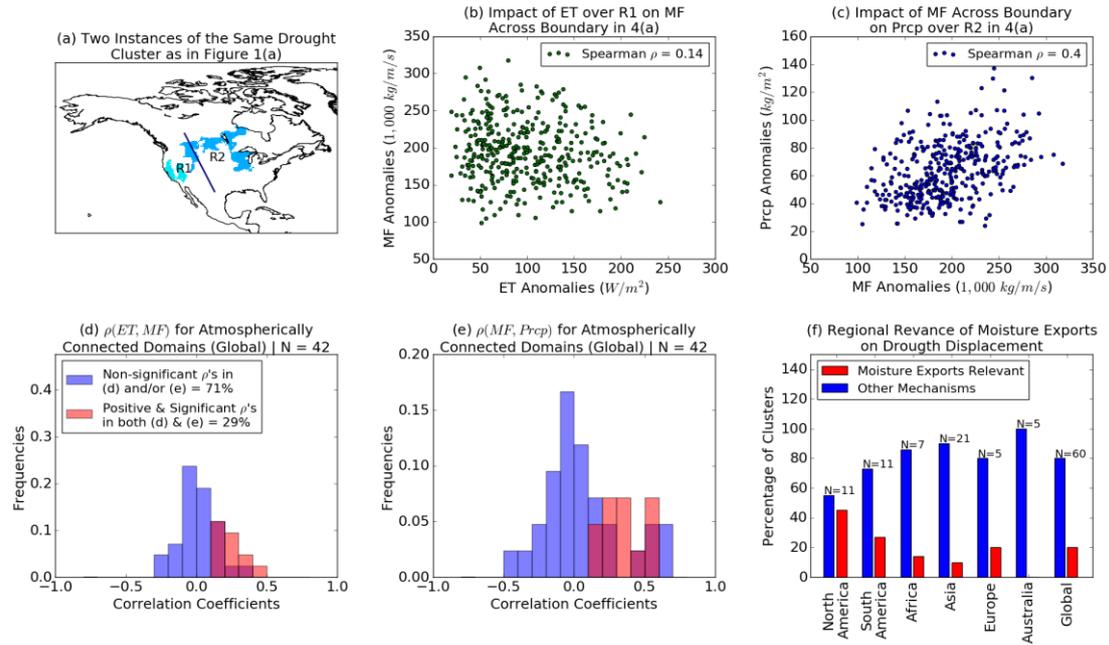
Figure 4. (a) Example of domains R1, R2, and the boundary between them. (b) Scatter plot and ρ between ET anomalies over R1 and MF across the boundary towards R2 shown in (a). (c) Similar to (b) for MF anomalies across the boundary and Prcp anomalies over R2. (d-e) Histograms of ρ's between ET and MF, and between MF and Prcp, respectively, for atmospherically connected domains. (f) Percentages of cases where the pair of correlations were positive and significant in each region.